J. Fluid Mech. (2025), *vol.* 1009, R6, doi:10.1017/jfm.2025.176



Small-scale anisotropy and ramp–cliff structures in turbulent shear flows

Xuechun Gong[1], **Ping-Fan Yang**[2,3], **Haitao Xu**[1] **and Alain Pumir**[4]

[1]Center for Combustion Energy and School of Aerospace Engineering, Tsinghua University, Beijing 100084, PR China

[2]School of Aeronautics and Institute of Extreme Mechanics, Northwestern Polytechnical University, Xi'an 710072, PR China

[3]National Key Laboratory of Aircraft Configuration Design, Xi'an 710072, PR China

[4]CNRS and Ecole Normale Supérieure de Lyon, Laboratoire de Physique, F-69342 Lyon, France

Corresponding author: Ping-Fan Yang, yangpingfan@nwpu.edu.cn

(Received 20 November 2024; revised 12 January 2025; accepted 3 February 2025)

Experimental and numerical observations in turbulent shear flows point to the persistence of the anisotropy imprinted by the large-scale velocity gradient down to the smallest scales of turbulence. This is reminiscent of the strong anisotropy induced by a mean passive scalar gradient, which manifests itself by the 'ramp–cliff' structures. In the shear flow problem, the anisotropy can be characterised by the odd-order moments of $\partial_y u$, where u is the fluctuating streamwise velocity component, and y is the direction of mean shear. Here, we extend the approach proposed by Buaria *et al.* (*Phys. Rev. Lett.*, 126, 034504, 2021) for the passive scalar fields, and postulate that fronts of width $\delta \sim \eta Re_\lambda^{1/4}$, where η is the Kolmogorov length scale, and Re_λ is the Taylor-based Reynolds number, explain the observed small-scale anisotropy for shear flows. This model is supported by the collapse of the positive tails of the probability density functions (PDFs) of $(\partial_y u)/(u'/\delta)$ in turbulent homogeneous shear flows (THSF) when the PDFs are normalised by δ/L, where u' is the root-mean-square of u and L is the integral length scale. The predictions of this model for the odd-order moments of $\partial_y u$ in THSF agree well with direct numerical simulation (DNS) and experimental results. Moreover, the extension of our analysis to the log-layer of turbulent channel flows (TCF) leads to the prediction that the odd-order moments of order $p (p > 1)$ of $\partial_y u$ have power-law dependencies on the wall distance y^+: $\langle(\partial_y u)^p\rangle/\langle(\partial_y u)^2\rangle^{p/2} \sim (y^+)^{(p-5)/8}$, which is consistent with DNS results.

Key words: homogeneous turbulence, turbulence theory, turbulent boundary layers

© The Author(s), 2025. Published by Cambridge University Press.

https://doi.org/10.1017/jfm.2025.176 Published online by Cambridge University Press

1. Introduction

The overwhelming majority of turbulent flows, relevant to natural or technological processes, is anisotropic due to the specificity of the motion at large scales, which may include a shear or a straining motion. In his seminal work, Kolmogorov (1941) postulated that at very high Reynolds numbers and far from boundaries, the statistical properties of turbulent motion at sufficiently small scales are isotropic, insensitive to the anisotropy imposed at the largest scales. This fundamental hypothesis of the theory of Kolmogorov (1941) (in short, K41) plays a crucial role for many subsequent turbulence theories and models. In practice, however, Reynolds numbers are large, but finite, leaving open the quantitative question of to what extent small scales are influenced by the flow properties at large -scale. Specifically, in turbulent shear flows, small-scale anisotropy can be characterised by the odd-order moments of $\partial_y u$, where u is the fluctuating streamwise velocity component and y is the direction of mean shear. The analyses of Corrsin (1958) and Lumley (1967) lead to the conclusion that as the Reynolds number increases, the skewness of $\partial_y u$ decays as Re_λ^{-1}, where $Re_\lambda \equiv u'\lambda/\nu$ is the Reynolds number based on the Taylor microscale $\lambda \equiv u'/\langle(\partial_x u)^2\rangle^{1/2}$, u' is the root-mean-square of the streamwise velocity u, and ν is the kinematic viscosity. The prediction, which also applies to the decay of anisotropy in passive scalar fluctuations in turbulent flow fields, was first challenged by experimental measurements of scalar statistics under the existence of a mean scalar gradient $\boldsymbol{G}$ (Tong & Warhaft 1994; Shraiman & Siggia 2000; Warhaft 2000), along with numerical studies of simplified models (Holzer & Siggia 1994) and direct numerical simulations (DNS) (Pumir 1994). These results together with more recent DNS results at much higher Re_λ (Buaria *et al.* 2021) clearly establish that the skewness of the fluctuating scalar gradient $\partial_l\theta = \boldsymbol{G}\cdot\nabla\theta/|\boldsymbol{G}|$ is $O(1)$ and persists as Re_λ increases, i.e. $S_{\partial_l\theta} \sim Re_\lambda^0$, casting doubt on the classical prediction of Re_λ^{-1}. This anomalous behaviour, which shows a clear violation of the anisotropy of the scalar field at the smallest scales in the flow, can be related to the presence of large-scale 'ramp–cliff' structures observed long ago (see e.g. Mestayer *et al.* 1976; Gibson *et al.* 1977; Sreenivasan *et al.* 1979; Mestayer 1982). These structures feature a wide 'ramp' region where the physical quantity changes gradually, followed by a 'cliff' region where changes are sharp. The anisotropy originates from a strong alignment of the scalar gradients in the cliff with the mean scalar gradient. Recently, Sreenivasan (2019) proposed a method to estimate the order of magnitude of $S_{\partial_l\theta}$ based on ramp–cliff structures in passive scalar fields. Based on this idea, Buaria *et al.* (2021) developed a model providing quantitative predictions for the Re_λ scaling of the odd-order moments of $\partial_l\theta$, which agree well with numerical results.

The study of small-scale anisotropy in scalar fields with a mean gradient has raised the question of whether similar behaviours occur in the turbulent velocity field with a mean shear $S \equiv \mathrm{d}\langle U\rangle/\mathrm{d}y$ (Pumir & Shraiman 1995; Casciola *et al.* 2003; Smits *et al.* 2011), where $\langle U\rangle$ is the mean velocity taken here to be varying only in the y-direction. For turbulent homogeneous shear flows (THSF) with a constant mean shear, experimental (Garg & Warhaft 1998; Ferchichi & Tavoularis 2000; Shen & Warhaft 2000; Warhaft & Shen 2001) and DNS results (Rogers 1986; Pumir 1996) have demonstrated that the skewness of $\partial_y u$, $S_3 \equiv \langle(\partial_y u)^3\rangle/\langle(\partial_y u)^2\rangle^{3/2}$, exhibits a weaker dependence on Re_λ that also differs from the classical prediction of Re_λ^{-1}, although less strongly than for the passive scalar. Flow visualisations demonstrate the presence of large-scale ramp–cliff structures in THSF (Pumir & Shraiman 1995). This suggests to apply the model proposed for the scalar (Buaria *et al.* 2021) also to the velocity fields in THSF. As we show here, this approach leads to quantitative predictions for small-scale anisotropy in velocity statistics, particularly the scaling of odd-order moments of $\partial_y u$ with Re_λ.

https://doi.org/10.1017/jfm.2025.176 Published online by Cambridge University Press

Furthermore, ramp–cliff structures also have close connections with the existence of uniform momentum zones observed in turbulent boundary layers (Meinhart & Adrian 1995). Additionally, the suggestive evidence for ramp–cliff structures in instantaneous streamwise velocity profiles of fully developed turbulent channel flows (TCF), especially in the inner region, are provided by Pumir *et al.* (2016). Meanwhile, a significant decay of S_3 with respect to the wall distance in the log-layer region has also been observed by Vreman & Kuerten (2014). Based on the similarities between THSF and TCF for both large (Sekimoto *et al.* 2016; Dong *et al.* 2017) and small scales (Pumir *et al.* 2016; Pumir 2017), we extend the discussions of small-scale anisotropy to TCF. This allows us to predict that the odd-order moments of $\partial_y u$ depend on the distance y to the wall as a power-law function.

The rest of the paper is organised as follows. In § 2, we briefly introduce the experimental and DNS data used in this work. Then in § 3, we review the model proposed by Buaria *et al.* (2021) for scalar fields and extend it to THSF to characterise the small-scale anisotropic properties of the odd-order moments of $\partial_y u$, and derive the scaling of the characteristic length scale of the cliff, δ, in THSF. In § 4, we generalise the discussions to the log-layer region of TCF and obtain how anisotropy decays as the distance from the wall increases. Finally, we summarise and conclude our findings in § 5.

2. Data used

The THSF data analysed in this work include both DNS and experimental data. Numerically, the Navier–Stokes equations are solved by DNS in a periodic domain by using the pseudo-spectral method developed by Rogallo (1981) to efficiently account for the shear. The code is described in Pumir & Shraiman (1995) and Pumir (1996). Physically, turbulence is maintained by the interaction between the mean shear and the velocity fluctuations, without any extra forcing. We chose a domain of size $4\pi \times 2\pi \times 2\pi$, following the work of Sekimoto *et al.* (2016), who showed that the corresponding THSF provide a good model for shear driven turbulence. Correspondingly, the system is discretised with $2M \times M \times M$ Fourier modes. To the simulations with $M = 100$ and $M = 160$, discussed in Pumir (2017) and Yang *et al.* (2021), we added here a new simulation with $M = 256$. The corresponding Reynolds numbers, defined by $Re_\lambda = \langle u^2\rangle/[\nu\langle(\partial_x u)^2\rangle^{1/2}]$, are $Re_\lambda = 120$, 145 and 230, respectively. Defining the Kolmogorov length as $\eta = (\nu^3/\varepsilon)^{1/4}$, where ν is viscosity and ε is the kinetic energy dissipation rate per unit mass, and k_{max} the largest mode faithfully represented in the simulation, the product $k_{max}\eta$ was $\gtrsim 1.3$. The total durations of the runs, T_{tot}, were equal to 720 S^{-1} ($M = 100$), 432 S^{-1} ($M = 160$) and 190 S^{-1} ($M = 256$).

For TCF, we used the DNS data from the Johns Hopkins Turbulence Databases (JHTDB). In this work, we mainly use the dataset with the Reynolds number $Re_\tau \equiv u_\tau h/\nu = 5200$ (Lee & Moser 2015), where $u_\tau \equiv \sqrt{\tau_w/\rho}$ is the friction velocity, h is the half-height of the channel, τ_w is the wall shear stress and ρ is the density of the fluid. The DNS of TCF are conducted within a rectangular domain of size 8π, 2 and 3π in the streamwise (x), wall-normal (y) and spanwise (z) directions, respectively. We downloaded data from the instantaneous velocity fields at $t = 0$, 1, …, 8 and 10, a total of 10 time instants. Pumir *et al.* (2016) pointed out that at $t = 9$, the skewness of $\partial_y u$ at the centre of the channel does not vanish, which is inconsistent with the requirement of symmetry. For this reason, we have not included the data at $t = 9$ in our analysis. From each velocity field, we selected 27 different wall-parallel (x–z) planes in both the upper and lower parts of the channel and downloaded $N_x \times N_z = 3200 \times 1200$ data points from each plane, resulting in $3200 \times 1200 \times 10 \times 2 \sim 7 \times 10^7$ samples at each wall distance. For comparison, we also

https://doi.org/10.1017/jfm.2025.176 Published online by Cambridge University Press

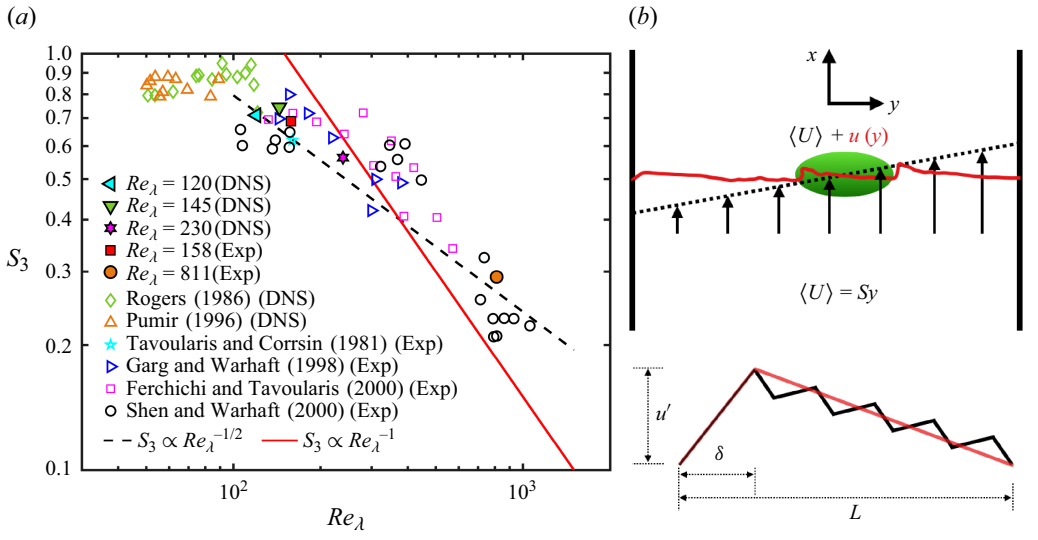


Figure 1. (*a*) Summarised experimental and numerical results for the skewness of $\partial_y u$ in THSF. The red solid line and the black dashed line indicate the Re_λ^{-1} and $Re_\lambda^{-1/2}$ scaling, respectively. (*b*) A sketch of the ramp–cliff structures in the instantaneous streamwise velocity profile for THSF, which is the sum of the mean velocity, $\langle U \rangle = Sy$ (dotted black line) and the fluctuation, $u(y)$ (solid red line), where S is the mean shear rate and y is the coordinate in the direction of the mean shear. The lower part shows the zoom-in of the instantaneous fluctuation velocity in the green region.

considered the lower Reynolds dataset with $Re_\tau = 1000$ (Graham *et al.* 2016). Similar to Pumir *et al.* (2016), we chose 10 snapshots at $t = 2.5 + t \times n$, $n = 0, \ldots, 9$, and from each snapshot we selected 47 $x-z$ planes from both sides of the channel and downloaded $\sim 2 \times 10^7$ at each wall distance.

The experimental results for $Re_\lambda = 158$ and $Re_\lambda = 811$ are from the hot-wire measurement in homogeneous shear flows in a wind tunnel by Shen & Warhaft (2000).

3. Ramp–cliff structures of velocity in THSF

The local isotropy assumption of the K41 theory states that when the Reynolds number Re_λ is sufficiently high, the influence of large-scale anisotropy on small scales is negligible. One of the consequences of local isotropy is that the odd-order moments of $\partial_y u$ should be approximately zero. The local isotropy hypothesis is typically investigated in idealised turbulent flows, such as THSF, which break isotropy but retain homogeneity. The lowest non-zero odd-order moment, the skewness S_3 of the THSF data from this work is shown in figure 1(*a*), together with numerical (Rogers 1986; Pumir 1996, 2017) and experimental (Tavoularis & Corrsin 1981; Garg & Warhaft 1998; Ferchichi & Tavoularis 2000; Shen & Warhaft 2000) data. Here, we consider the possibility of a relation between the scaling of the skewness as $S_3 \sim Re_\lambda^{-1/2}$ (Shen & Warhaft 2000), and the ramp–cliff structures observed in the velocity field of THSF from DNS (Pumir & Shraiman 1995), similar to what had been studied in the case of a passive scalar (Buaria *et al.* 2021). For this reason, we briefly review the model proposed by Buaria *et al.* (2021) for passive scalar fields and then extend it to the THSF.

Buaria *et al.* (2021) estimated that the odd-order moments of the partial derivative of θ in the direction parallel to the imposed scalar mean gradient are dominated by contributions from the 'cliff' sides of the ramp–cliff structures, where the scalar jumps by $\sim \theta' \equiv \langle \theta^2 \rangle^{1/2}$

https://doi.org/10.1017/jfm.2025.176 Published online by Cambridge University Press

over a very short scale δ_θ and thus occupies a fraction of δ_θ/L. This leads to

$$\langle(\partial_l\theta)^p\rangle \sim \left(\frac{\theta'}{\delta_\theta}\right)^p \frac{\delta_\theta}{L}. \tag{3.1}$$

Quantitative predictions then rely on the correct estimation of δ_θ. For passive scalars, δ_θ is controlled by the competition between diffusion and turbulent advection. The extension of these ideas to the THSF problem requires some care: judging from the difference in the power laws for $S_{\partial_l\theta} \sim Re_\lambda^0$ and $S_3 \sim Re_\lambda^{-1/2}$, very different length scales are involved for the scalar and for the velocity fields. Therefore, our next step is to determine this length scale.

As sketched in figure 1(*b*), the size of the entire ramp–cliff structure in the velocity field is of the order of the integral length scale L, while the cliff occupies a much smaller scale δ, within which significant variations in streamwise velocity occur with a typical magnitude of u'. Therefore, the typical value of $\partial_y u$ in the cliff region is u'/δ, and the fraction of the cliff region is proportional to δ/L; while in the ramp region these are u'/L and $1-(\delta/L)$, respectively. Since $\delta \ll L$, for odd orders $p = 3, 5, \ldots$, the contribution to the moments $\langle(\partial_y u)^p\rangle$ from the cliff regions can be estimated as

$$\langle(\partial_y u)^p\rangle \sim \left(\frac{u'}{\delta}\right)^p \frac{\delta}{L}, \tag{3.2}$$

while the contribution from the ramp regions is negligible in comparison. Letting $p = 3$ and normalising (3.2) by $\langle(\partial_y u)^2\rangle^{3/2}$, we obtain a prediction for S_3:

$$S_3 \equiv \frac{\langle(\partial_y u)^3\rangle}{\langle(\partial_y u)^2\rangle^{3/2}} \sim \left(\frac{u'}{\delta}\right)^3 \frac{\delta}{L} \Big/ \left(\frac{\varepsilon}{\nu}\right)^{3/2} \sim \frac{\nu^{3/2}}{\delta^2\varepsilon^{1/2}} \sim \left(\frac{\eta}{\delta}\right)^2. \tag{3.3}$$

In the steps earlier, we used the relation between the turbulent dissipation rate and the velocity derivatives, $\varepsilon \sim \nu\langle(\partial_y u)^2\rangle$; the so-called zeroth law of turbulence, $u'^3/L \sim \varepsilon$; and the definition of the Kolmogorov scale $\eta \equiv (\nu^3/\varepsilon)^{1/4}$, respectively. The empirical relation $S_3 \sim Re_\lambda^{-1/2}$, see figure 1(*a*), thus leads to the conclusion that the characteristic cliff size behaves as

$$\delta \sim Re_\lambda^{1/4}\eta. \tag{3.4}$$

We stress that the scaling of the length scale δ in the cliff region has been obtained solely from the scaling of the lowest non-trivial odd-order moment, namely the skewness S_3. Whether the length scale δ defined by (3.4) correctly provides an accurate description of higher-order moments such as S_5 and S_7, requires further testing. To this end, we focus on the large positive events of $\partial_y u$, and more specifically on the positive tails of the probability density functions (PDF) of $\partial_y u$, since the cliff regions dominate the contribution to the large positive events of $\partial_y u$. Figure 2(*a*) shows the PDFs of $\partial_y u$ normalised by the root-mean-square value $\langle(\partial_y u)^2\rangle^{1/2}$. These PDFs are collected from various sources, including two experimental cases with $Re_\lambda = 158$ and $Re_\lambda = 811$ from Shen & Warhaft (2000), as well as three DNS cases with $Re_\lambda = 120$, $Re_\lambda = 145$ (Pumir 2017) and $Re_\lambda = 230$. We observe that as the Reynolds number increases, the positive tails extend further, albeit not as rapidly as the negative ones, which is consistent with the decrease in the skewness S_3 when Re_λ increases, as shown by figure 1(*a*).

On the other hand, the positive tails of the PDFs should collapse if we choose the assumed characteristic scale of the velocity gradient in these regions, u'/δ, to normalise the $\partial_y u$ and use δ/L to normalise the values of the PDFs. Noting that $u'^3/L \sim \varepsilon$,

https://doi.org/10.1017/jfm.2025.176 Published online by Cambridge University Press

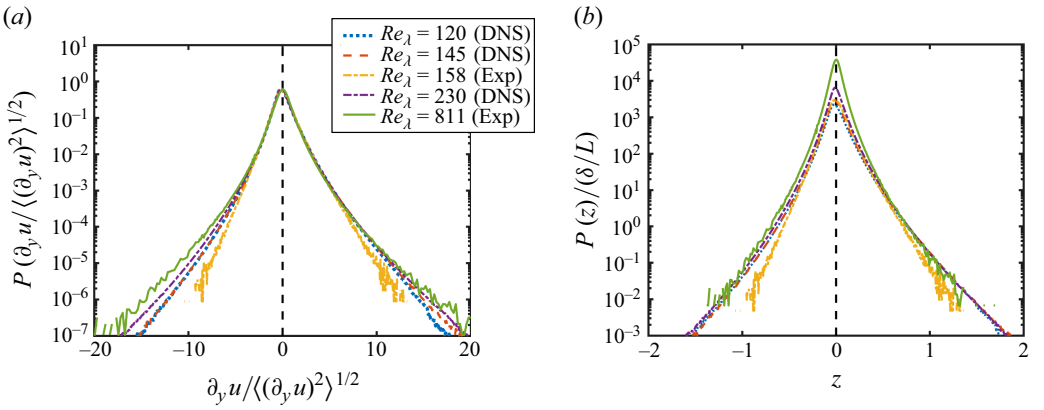


Figure 2. The PDFs of the velocity derivative $\partial_y u$ from DNS ($Re_\lambda = 120$, $Re_\lambda = 144$ and $Re_\lambda = 230$) and experiments ($Re_\lambda = 158$ and $Re_\lambda = 811$, see Shen & Warhaft 2000). Panel (*a*) shows $\partial_y u$ normalised by its root-of-mean values. Panel (*b*) shows $\partial_y u$ normalised by u'/δ ($z \equiv \partial_y u/(\langle(\partial_y u)^2\rangle^{1/2} Re_\lambda^{1/4})$). The PDFs are normalised by δ/L according to (3.5).

$L/\eta \sim Re_\lambda^{3/2}$ and $\varepsilon \sim \nu\langle(\partial_y u)^2\rangle$, one obtains from (3.4)

$$u'/\delta \sim \langle(\partial_y u)^2\rangle^{1/2} Re_\lambda^{1/4}, \quad \delta/L \sim Re_\lambda^{-5/4}, \tag{3.5}$$

which allows us to determine the normalisation factors from the known data and thus provides a convenient way to transfer the normalisation in figure 2(*a*) to the normalisations by u'/δ and δ/L. Figure 2(*b*) shows the PDFs of the rescaled velocity derivative $z \equiv \partial_y u/(\langle(\partial_y u)^2\rangle^{1/2} Re_\lambda^{1/4})$, with the values of PDFs, $P(z)$, normalised by $Re_\lambda^{-5/4}$. Figure 2(*b*) suggests a generally good collapse of the positive tails for different Re_λ from both DNS and experiments, aside for the experimental data at $Re_\lambda = 158$, which may be attributed to the limited number of statistics in this case compared with the other datasets. The collapse of the positive tails of the rescaled PDFs can be quantitatively evaluated by taking the ratios of the PDF curves at different Reynolds numbers. The ratio analysis (not shown) was performed for the DNS cases at two Reynolds numbers and indicated that these ratios indeed exhibit a plateau near one in the region of $z \gtrsim O(1)$, corresponding to the large positive derivatives. The collapse supports that the large positive events of $\partial_y u$ indeed scale as u'/δ with a probability proportional to δ/L.

Using the expression for δ, (3.4), and substituting into (3.2), one obtains the scaling of the normalised pth odd-order moments of the streamwise velocity derivative $\partial_y u$, S_p as a function of Re_λ:

$$S_p \equiv \frac{\langle(\partial_y u)^p\rangle}{\langle(\partial_y u)^2\rangle^{p/2}} \sim Re_\lambda^{(p-5)/4}. \tag{3.6}$$

Specifically, the cases for $p = 5, 7$ correspond to $S_5 \equiv \langle(\partial_y u)^5\rangle/\langle(\partial_y u)^2\rangle^{5/2}$ and $S_7 \equiv \langle(\partial_y u)^7\rangle/\langle(\partial_y u)^2\rangle^{7/2}$, respectively. The prediction from (3.6) for S_5 is $S_5 \sim Re_\lambda^0$, which agrees very well with the experimental result of $\sim Re_\lambda^{-0.02}$ in Shen & Warhaft (2000). The prediction for $S_7 \sim Re_\lambda^{0.5}$ is not inconsistent with the data of Shen & Warhaft (2000) and Warhaft & Shen (2001), which reported $S_7 \sim Re_\lambda^{0.63}$, considering the scatter of the data (see e.g. figure 11 of Shen & Warhaft 2000). Notably, our model predicts that the normalised odd-order moments S_p with $p \geqslant 5$ do not decay towards zero as $Re_\lambda \to \infty$, which clearly are not in favour of the assumption of return to isotropy.

https://doi.org/10.1017/jfm.2025.176 Published online by Cambridge University Press

We note that in the analysis earlier, we have assumed that the exponent of the scaling of S_3 as a function of Re_λ is $-1/2$, which differs slightly from the scaling of $S_3 \sim Re_\lambda^{-0.52}$ proposed by Shen & Warhaft (2000). A straightforward analysis shows that the collapse of the normalised PDFs is robust under small changes in the exponents.

The earlier results substantiate the close relation between the odd-order moments of $\partial_y u$ and the ramp–cliff structures in THSF. They provide the motivation for exploring further their relations in more complex shear flows such as TCF.

4. The anisotropy of velocity gradients in TCF

One of the conditions for the turbulent flow to restore isotropy in K41 theory is that the Reynolds number should be sufficiently high, as explained in § 3. The other requirement for local isotropy at small scales is that the flow is far enough from any boundary. Therefore, in wall-bounded shear turbulence, with the presence of a wall, an important question is the dependence of small-scale anisotropy on the distance to the wall (i.e. the wall distance y). Specifically, we ask whether the odd-order moments of $\partial_y u$ diminish as y increases in TCF. In near-wall turbulence, the dimensionless wall distance $y^+ \equiv y/\delta_\nu = u_\tau y/\nu$ is the physical distance to the wall measured in units of the thickness of the viscous sublayer $\delta_\nu \equiv \nu/u_\tau$ (see e.g. Pope 2000). Consequently, y^+ can also be regarded as an effective local Reynolds number representing the scale separation between the local integral scale and the viscous scale at that particular position. For this reason, we expect that in the log-layer region where $y^+ \gg 1$ and $y/h \ll 1$, the behaviour of the odd-order moments of $\partial_y u$ should show similarities to the case of THSF, which may also not support the return to isotropy assumption (Pumir & Shraiman 1995).

It has been observed that normalised third-order moment S_3 decreases as y^+ increases in the log-layer region (Vreman & Kuerten 2014; Pumir *et al.* 2016). However, a quantitative description of the y^+ dependence of S_3, or of the higher-moments such as S_5 and S_7, is not available. Pumir *et al.* (2016) also observed large-scale ramp–cliff structures in the instantaneous streamwise velocity field in TCF. This is also consistent with the existence of uniform streamwise momentum regions in boundary layers (Meinhart & Adrian 1995). These observations encourage us to generalise the discussions from the last section on THSF to the odd-order moments S_p $(p > 1)$ in TCF. This is particularly relevant for predicting the y^+ scaling of S_p in the log-layer region.

As before, we assume that the cliff regions dominate the contribution to the odd-order moments of $\partial_y u$ and generalise (3.2) to the log-layer of TCF. To estimate the typical length scale δ of the cliff regions and its y^+ dependence, we assume that δ still satisfies (3.4) locally, i.e. $\delta \sim Re_\lambda^{1/4}\eta$ at any given y^+ by making the analogy that the ramp–cliff structures in TCF are similar to those in THSF at the same local Reynolds number. Next, we need to estimate the y^+ dependence of Re_λ and η in the log-layer of TCF. From the definition of Re_λ and noticing that in the log-layer the fluctuation velocity u' is nearly constant (Pope 2000) and the balance between local production and dissipation leads to $\varepsilon \sim \nu\langle(\partial_x u)^2\rangle \propto (y^+)^{-1}$ (Pumir *et al.* 2016; Li *et al.* 2024), we have

$$Re_\lambda \equiv \frac{u'^2}{\nu\langle(\partial_x u)^2\rangle^{1/2}} \sim \frac{1}{\nu\langle(\partial_y u)^2\rangle^{1/2}} \sim (y^+)^{1/2}. \tag{4.1}$$

Meanwhile, since $\varepsilon \sim (y^+)^{-1}$, the Kolmogorov length η scales as

$$\eta \equiv \nu^{3/4}\varepsilon^{-1/4} \sim (y^+)^{1/4}. \tag{4.2}$$

https://doi.org/10.1017/jfm.2025.176 Published online by Cambridge University Press

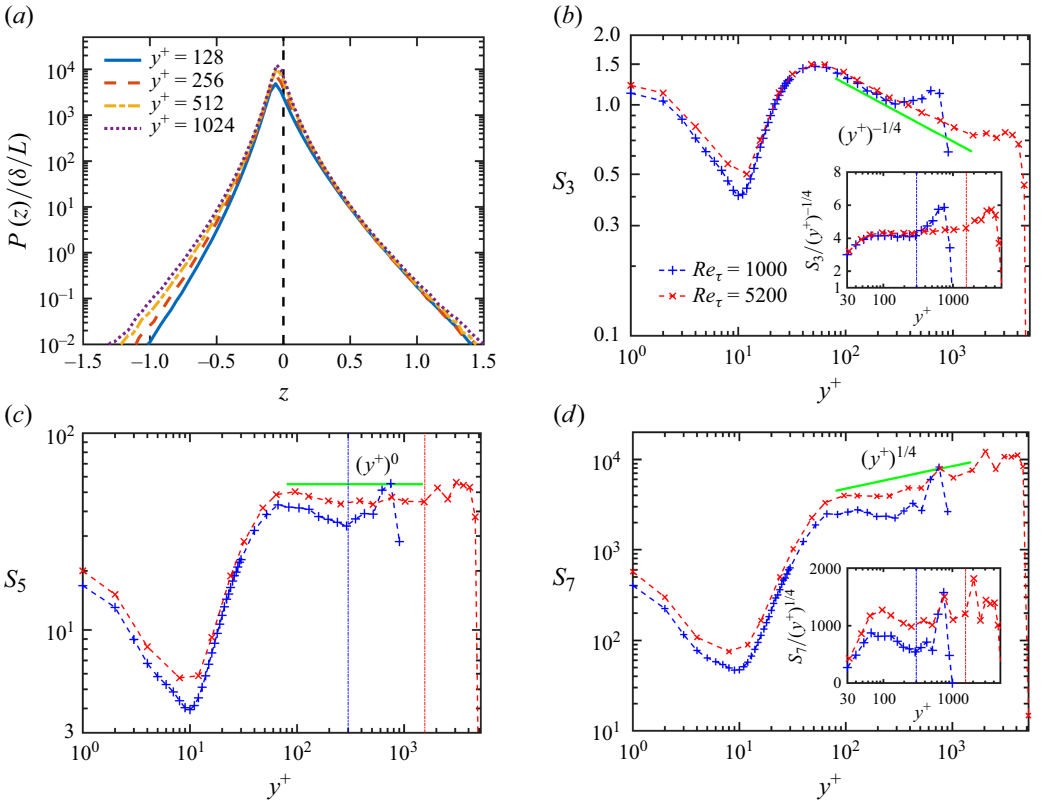


Figure 3. (*a*) The PDFs of $\partial_y u$ scaled by u'/δ and δ/L using the expression of (3.5) at $y^+ = 128$, 256, 512 and 1024 in the log-layer of the TCF with the Reynolds number $Re_\tau = 5200$. (*b–d*) The variations of normalised odd-order moments S_3, S_5 and S_7 of $\partial_y u$ in TCF at two Reynolds numbers, $Re_\tau = 1000$ (blue plus symbols) and $Re_\tau = 5200$ (red cross symbols). The green solid lines illustrate predictions by (4.5). The curves in the insets of (*b*) and (*d*) are compensated by corresponding y^+-scaling expressed in (4.6) in the log-layer region. Vertical dash-dotted lines in (*b–d*) mark the upper bounds of the log-layer region at the two Reynolds numbers.

Then from (4.1) and (4.2) we obtain

$$\delta \sim Re_\lambda^{1/4}\eta \sim (y^+)^{3/8}. \tag{4.3}$$

In § 3 (figure 2*b*) we observed that normalising $\partial_y u$ and its PDF values respectively by u'/δ and δ/L can collapse the positive tails of the PDFs of $\partial_y u$ in THSF. Figure 3(*a*) generalises this approach to the PDFs of $\partial_y u$ at different positions in the log-layer of TCF. Namely, figure 3(*a*) shows the PDFs of $\partial_y u$ normalised according to (3.5) with the local $\langle(\partial_y u)^2\rangle^{1/2}$ and Re_λ determined from their definitions at four different positions $y^+ = 128$, 256, 512 and 1024 in the log-layer of the TCF at $Re_\tau = 5200$. The positive tails of the PDFs at different y^+ collapse very well, supporting our assumption that the large positive events of $\partial_y u$ in the log-layer of TCF are indeed dominated by cliff structures, with a typical scale of u'/δ and probability δ/L, similar to the case in THSF. Based on this observation, we can further discuss the y^+ dependence of the normalised odd-order moments of $\partial_y u$, S_p, within the log-layer region.

In addition to the scaling of Re_λ, η and δ shown in (4.1)–(4.3), to predict the scaling of S_p using (3.2), we still need to determine the y^+ dependence of the integral length scale L. We note that near the wall, L is controlled by the largest eddy allowed by the

https://doi.org/10.1017/jfm.2025.176 Published online by Cambridge University Press

distance to the wall, i.e.

$$L \sim y^+. \tag{4.4}$$

Combining these results from (4.1) to (4.4), we obtain

$$S_p \equiv \frac{\langle (\partial_y u)^p \rangle}{\langle (\partial_y u)^2 \rangle^{p/2}} \sim (y^+)^{(p-5)/8}. \tag{4.5}$$

For the specific values of $p = 3$, 5 and 7, the predictions are

$$S_3 \sim (y^+)^{-1/4}, \quad S_5 \sim (y^+)^0, \quad S_7 \sim (y^+)^{1/4}. \tag{4.6}$$

Figures 3(*b*) and 3(*d*) present the y-dependence of S_3, S_5 and S_7 in TCF at two different Reynolds numbers. $Re_\tau = 5200$ and $Re_\tau = 1000$. For a better comparison between the results from these two data sets and our predictions, insets in figures 3(*b*) and 3(*d*) show these odd-order moments compensated by the corresponding y^+-scaling given by (4.6). It can be seen that the results for the skewness S_3 are consistent with a power-law decay in the log-layer region as y^+ increases until the centre region ($y/h \geqslant 0.3$) is reached, where the skewness hits a plateau, before going to zero at the centre of the channel due to symmetry requirement. We notice that for $Re_\tau = 1000$, the log-layer is very narrow. By performing a least-squares fit on the $Re_\tau = 5200$ data over the range $60 < y^+ < 1024$, we obtain a scaling of $S_3 \sim (y^+)^{-0.22}$, which is consistent with the prediction of $(y^+)^{-1/4}$ by (4.6). We also observe that the normalised fifth-order moment S_5 is nearly constant in figure 3(*c*), and the seventh-order moment shows an approximate scaling of $S_7 \sim (y^+)^{1/4}$ in the log-layer region in figure 3(*d*), consistent with the predictions by (4.6). In summary, (4.5), derived by stressing the role of the ramp–cliff structures, agrees with DNS results at least for the odd-order moments S_p with $p \leqslant 7$. These results suggest that in the log-layer of TCF, the large positive events of $\partial_y u$ are also predominantly contributed by cliff structures, extending our understanding of small-scale anisotropy from the simple THSF to the more complex case with the presence of a wall.

5. Conclusion

In conclusion, we propose that in turbulent shear flows, the ramp–cliff structures induced by the large-scale mean shear provide the dominant contribution to the small-scale anisotropy, which can be captured quantitatively by generalising the model proposed by Buaria *et al.* (2021) to the velocity fields in turbulent shear flows and specifying the typical length scale of the cliff structures as $\delta \sim {Re_\lambda}^{1/4}\eta$. When normalised accordingly, the positive tails of the PDFs of $\partial_y u$ collapse well, which provides support to our model and confirms that the large positive events of $\partial_y u$ scale as u'/δ with a probability proportional to δ/L. The model then predicts the Reynolds number dependence of the odd-order moments of $\partial_y u$, which is in good agreement with the available experimental and numerical results. Specifically, the model explains the observation that the normalised odd-order moments S_p with $p > 3$ do not decay to zero as the Reynolds number increases, which contradicts the assumption of return to isotropy. Furthermore, we extend the discussion to the log-layer of TCF, where we identified a power-law scaling for the odd-order moments of $\partial_y u$ versus the wall distance y^+: $\langle (\partial_y u)^p \rangle / \langle (\partial_y u)^2 \rangle^{p/2} \sim (y^+)^{(p-5)/8}$, and compared it with high-Reynolds-number DNS data. In summary, this study not only substantiates the existence of ramp–cliff structures in turbulent shear flows but also elucidates the typical length scale of the cliff region, where the effects of small-scale anisotropy are most pronounced. A challenging question for further study is to provide a theoretical explanation for the scaling of δ. Furthermore, it would be interesting to

https://doi.org/10.1017/jfm.2025.176 Published online by Cambridge University Press

extend the ideas presented in this work to other free shear flows, such as wakes or jets. Our preliminary analysis of the turbulent axisymmetric round-jet data measured by Peng *et al.* (2023) suggests that the ramp–cliff structures also exist in the velocity fields of the free shear flows.

Acknowledgements. We are grateful to X. Shen and Z. Warhaft for making the original data from Shen & Warhaft (2000) available for us to show in figure 2. We also thank H. Xi and his group for sharing their turbulent axisymmetric round-jet data for our preliminary analysis.

Funding. X.G., P.F.Y. and H.X. acknowledge support from the National Natural Science Foundation of China (NSFC) under grants 12202452, 11672157, 91852104 and 11988102, and the Fundamental Research Funds for Central University (no. D5000240110). A.P. was supported by the French Agence Nationale de la Recherche under contract no. ANR-20-CE 30-0035 (project TILT), and acknowledges the Max-Planck Institut for Dynamics and Self-Organisation.

Declaration of interests. The authors report no conflict of interest.

References

Buaria, D., Clay, M.P., Sreenivasan, K.R. & Yeung, P.K. 2021 Small-scale isotropy and ramp-cliff structures in scalar turbulence. *Phys. Rev. Lett.* **126** (3), 034504.

Casciola, C.M., Gualtieri, P., Benzi, R. & Piva, R. 2003 Scale-by-scale budget and similarity laws for shear turbulence. *J. Fluid Mech.* **476**, 105–114.

Corrsin, S. 1958 Local isotropy in turbulent shear flow. *NACA Tech. Rep.* RM 58B11.

Dong, S., Lozano-Durán, A., Sekimoto, A. & Jiménez, J. 2017 Coherent structures in statistically stationary homogeneous shear turbulence. *J. Fluid Mech.* **816**, 167–208.

Ferchichi, M. & Tavoularis, S. 2000 Reynolds number effects on the fine structure of uniformly sheared turbulence. *Phys. Fluids* **12** (11), 2942–2953.

Garg, S. & Warhaft, Z. 1998 On the small scale structure of simple shear flow. *Phys. Fluids* **10** (3), 662–673.

Gibson, C.H., Friehe, C.A. & McConnell, S.O. 1977 Structure of sheared turbulent fields. *Phys. Fluids* **20** (10), S156–S167.

Graham, J., *et al.* 2016 A web services accessible database of turbulent channel flow and its use for testing a new integral wall model for LES. *J. Turbul.* **17** (2), 181–215.

Holzer, M. & Siggia, E.D. 1994 Turbulent mixing of a passive scalar. *Phys. Fluids* **6** (5), 1820–1837.

Kolmogorov, A.N. 1941 The local structure of turbulence in incompressible viscous fluid for very large Reynolds number. *Dokl. Akad. Nauk SSSR* **30**, 301–305.

Lee, M. & Moser, R.D. 2015 Direct numerical simulation of turbulent channel flow up to $Re_\tau \approx 5200$. *J. Fluid Mech.* **774**, 395–415.

Li, X.X., Hu, R.F. & Fang, L. 2024 Scaling laws of velocity gradient moments of attached eddies. *Phys. Rev. Fluids* **9** (9), 094602.

Lumley, J.L. 1967 Similarity and the turbulent energy spectrum. *Phys. Fluids* **10** (4), 855–858.

Meinhart, C.D. & Adrian, R.J. 1995 On the existence of uniform momentum zones in a turbulent boundary layer. *Phys. Fluids* **7** (4), 694–696.

Mestayer, P. 1982 Local isotropy and anisotropy in a high-Reynolds-number turbulent boundary layer. *J. Fluid Mech.* **125**, 475–503.

Mestayer, P.G., Gibson, C.H., Coantic, M.F. & Patel, A.S. 1976 Local anisotropy in heated and cooled turbulent boundary layers. *Phys. Fluids* **19** (9), 1279–1287.

Peng, S.H., Zhang, Y.B. & Xi, H.D. 2023 Effects of polymer additives on the entrainment of turbulent water jet. *Phys. Fluids* **35** (4), 045110.

Pope, S.B. 2000 *Turbulent Flows*. Cambridge University Press.

Pumir, A. 1994 A numerical study of the mixing of a passive scalar in three dimensions in the presence of a mean gradient. *Phys. Fluids* **6** (6), 2118–2132.

Pumir, A. 1996 Turbulence in homogeneous shear flows. *Phys. Fluids* **8** (11), 3112–3127.

Pumir, A. 2017 Structure of the velocity gradient tensor in turbulent shear flows. *Phys. Rev. Fluids* **2** (7), 074602.

Pumir, A. & Shraiman, B.I. 1995 Persistent small scale anisotropy in homogeneous shear flows. *Phys. Rev. Lett.* **75** (17), 3114–3117.

Pumir, A., Xu, H. & Siggia, E.D. 2016 Small-scale anisotropy in turbulent boundary layers. *J. Fluid Mech.* **804**, 5–23.

https://doi.org/10.1017/jfm.2025.176 Published online by Cambridge University Press

ROGALLO, R.S. 1981 Numerical experiments in homogeneous turbulence. *NASA Tech. Rep.* 81315.

ROGERS, M.M. 1986 *The Structure and Modeling of the Hydrodynamic and Passive Scalar Fields in Homogeneous Turbulent Shear Flow*. Stanford University.

SEKIMOTO, A., DONG, S. & JIMÉNEZ, J. 2016 Direct numerical simulation of statistically stationary and homogeneous shear turbulence and its relation to other shear flows. *Phys. Fluids* **28** (3), 035101.

SHEN, X. & WARHAFT, Z. 2000 The anisotropy of the small scale structure in high Reynolds number ($R_\lambda \sim 1000$) turbulent shear flow. *Phys. Fluids* **12**, 2976–2989.

SHRAIMAN, B.I. & SIGGIA, E.D. 2000 Scalar turbulence. *Nature* **405** (6787), 639–646.

SMITS, A.J., MCKEON, B.J. & MARUSIC, I. 2011 High-Reynolds number wall turbulence. *Annu. Rev. Fluid Mech.* **43** (1), 353–375.

SREENIVASAN, K.R. 2019 Turbulent mixing: a perspective. *Proc. Natl Acad. Sci. USA* **116** (37), 18175–18183.

SREENIVASAN, K.R., ANTONIA, R.A. & BRITZ, D. 1979 Local isotropy and large structures in a heated turbulent jet. *J. Fluid Mech.* **94** (4), 745–775.

TAVOULARIS, S. & CORRSIN, S. 1981 Experiments in nearly homogeneous turbulent shear flow with a uniform mean temperature gradient. Part 2. The fine structure. *J. Fluid Mech.* **104**, 349–367.

TONG, C. & WARHAFT, Z. 1994 On passive scalar derivative statistics in grid turbulence. *Phys. Fluids* **6** (6), 2165–2176.

VREMAN, A.W. & KUERTEN, J.G.M. 2014 Statistics of spatial derivatives of velocity and pressure in turbulent channel flow. *Phys. Fluids* **26** (8), 085103.

WARHAFT, Z. 2000 Passive scalars in turbulent flows. *Annu. Rev. Fluid Mech.* **32** (1), 203–240.

WARHAFT, Z. & SHEN, X. 2001 Some comments on the small scale structure of turbulence at high Reynolds number. *Phys. Fluids* **13** (5), 1532–1533.

YANG, P.F., PUMIR, A. & XU, H. 2021 Return to isotropy of homogeneous shear-released turbulence. *Phys. Rev. Fluids* **6** (4), 044601.

https://doi.org/10.1017/jfm.2025.176 Published online by Cambridge University Press